Acta Crystallographica Section D
Biological Crystallography
ISSN 0907-4449

Structures of V45E and V45Y mutants and structure comparison of a variety of cytochrome b_5 mutants

Jian-Hua Gan,[a] Jian Wu,[a]† Zhi-Qiang Wang,[b] Yun-Hua Wang,[b] Zhong-Xian Huang[b]‡ and Zong-Xiang Xia[a]*‡

[a]State Key Laboratory of Bioorganic and Natural Products Chemistry, Shanghai Institute of Organic Chemistry, Chinese Academy of Sciences, Shanghai 200032, People's Republic of China, and [b]Chemical Biology Laboratory, Department of Chemistry, Fudan University, Shanghai 200433, People's Republic of China

† Present address: Department of Chemistry and Biochemistry, University of California at San Diego, San Diego, CA 92093, USA.
‡ Zong-Xiang Xia was in charge of the structure study and Zhong-Xian Huang was in charge of the preparation of the mutants and the determination of the protein properties.

Correspondence e-mail: xiazx@pub.sioc.ac.cn

Received 11 February 2002
Accepted 5 June 2002

PDB References: V45E, 1lqx, r1lqxsf; V45Y, 1lr6, r1lr6sf.

Val45 is a highly conserved residue and a component of the heme-pocket wall of cytochrome b_5. The crystal structures of cytochrome b_5 mutants V45E and V45Y have been determined at high resolution. Their overall structures were very similar to that of the wild-type protein. However, Val45 of the wild-type protein points towards the heme, but the large side chains of both Glu45 and Tyr45 of the mutants point towards the solvent. A channel is thus opened and the hydrophobicity of the heme pocket is decreased. The rotation of the porphyrin ring and the conformational change of the axial ligand His39 in the V45Y mutant indicate that the microenvironment of the heme is disturbed because of the mutation. The binding constants and the electron-transfer rates between cytochrome b_5 and cytochrome c decrease owing to the mutation, which can be accounted for by molecular modeling: the inter-iron distances increase in order to eliminate the unreasonably close contacts resulting from the large volumes of the mutated side chains. The influence of the mutations on the redox potentials and protein stability is also discussed. The structures of seven mutants of cytochrome b_5 are compared with each other and the effects of these mutations on the protein properties and functions are summarized.

1. Introduction

Cytochrome b_5 is a membrane-bound protein existing widely in biological systems. It is involved in a variety of electron-transfer processes, such as the desaturation of fatty acids as well as the reduction of cytochrome *P*450 and methemoglobin. The proteolysis of microsomal cytochrome b_5 produces a soluble fragment containing the prosthetic group heme and exhibiting the biological function of the intact membrane protein (Mathews, 1985; Mathews *et al.*, 1979).

The crystal structures of both the lipase-solubilized fragment and the recombinant trypsin-solubilized fragment of cytochrome b_5 were determined at high resolution (Durley & Mathews, 1996; Wu *et al.*, 2000), which provide the detailed structural basis for studying the structure–function relationship. Recently, the technique of site-directed mutagenesis was used to investigate the specific role played by various key residues of cytochrome b_5.

The trypsin-solubilized fragment of cytochrome b_5 is referred to as Tb_5 and contains 84 amino-acid residues (Ala3–Lys86). Heme is bound in a hydrophobic pocket with the wall and the bottom composed of four α-helices (helices II, III, IV and V) and three β-strands (β-strands II, III and IV), respectively. Val45 is a conserved residue located in α-helix III, which is a component residue of the pocket wall and makes van der Waals interactions with heme. Val45 is expected to be a key residue of cytochrome b_5. Some mutants

Table 1
Data-collection and crystallographic refinement statistics.

Values in parentheses correspond to the data for the highest resolution shell (1.80–1.84 Å for V45E and 1.90–1.94 Å for V45Y).

	V45E	V45Y
Resolution (Å)	1.8	1.9
No. of unique reflections	9048	7563
R_{sym}† (%)	5.1 (21.9)	6.2 (19.4)
Data completeness (%)	93.6 (74.5)	93.5 (76.3)
$\langle I/\sigma(I)\rangle$‡	19.6 (5.7)	14.3 (6.1)
Data with $I > 3\sigma(I)$ (%)	85.9 (53.4)	82.1 (52.7)
Multiplicity§	3.2 (2.5)	3.1 (2.3)
No. of amino-acid residues	82	82
No. of prosthetic groups	1	1
No. of solvent molecules	68	90
R factor (%)	18.9	19.2
Free *R* factor (%)	22.2	23.5
R.m.s.d.¶		
Bond lengths (Å)	0.010	0.008
Bond angles (°)	1.081	1.165
Mean temperature factors (Å^2)		
Main chain	20.77	23.28
Side chain	24.84	27.93
Heme	22.43	23.71
Solvent	24.37	27.46

† $R_{sym} = \sum|I - \langle I\rangle|/\sum I$. ‡ Mean signal-to-noise ratio. § The average number of measurements for each reflection used to calculate R_{sym}. ¶ Root-mean-square deviation

of Tb_5 at this residue were prepared in our laboratory by site-directed mutagenesis and the effects of the mutations at Val45 on the protein stability and redox potentials have been reported previously (Wang *et al.*, 2000). Cytochrome *c* is the electron acceptor of cytochrome b_5. The determination of the inter-protein binding constants of these mutants with cytochrome *c* and the electron-transfer rates will be published elsewhere in detail. To further understand the structural basis of the effects of the mutations on the protein properties and functions we present in this paper the crystal structures of two of the mutants, V45E and V45Y, and discuss the structure–function relationship revealed by these two mutants.

Val61 is another key residue, located at α-helix IV, and is also a component residue of the heme-pocket wall and makes van der Waals interactions with heme. Both Val45 and Val61 are located at the edge of the heme pocket but at the opposite sides of the heme plane. The crystal structure of the V61H mutant and the effects of this mutation on the structure and properties have been reported previously (Wu *et al.*, 2000). Phe35 and Pro40 are two of the component residues of a hydrophobic patch on the molecular surface; Phe35 is located at α-helix II and Pro40 immediately follows this helix. The crystal structures of F35Y and P40V were also determined and the structure–function relationship has been studied (unpublished results). The mutation sites of the five mutants F35Y, P40V, V45E, V45Y and V61H all surround the heme prosthetic group, as shown in Fig. 1.

A different type of mutant was also prepared in our laboratory. Glu44, Glu48, Glu56 and Asp60 are negatively charged residues located at the molecular surface (Fig. 1) and are involved in the inter-protein interactions with cytochrome *c* (Salemme, 1976; Northrup *et al.*, 1993). The crystal structures of two mutants of this type have been determined, one in which two (Glu44 and Glu56) and the other in which all four residues were mutated to non-polar alanine residues. (The quadruple-site mutant is referred to as Mut4.) The mutations lead to little change in the structure (unpublished results).

The crystal structures of the seven mutants and the wild-type Tb_5 were all determined at high resolution and a structure comparison is presented in this paper. The effects of these mutations on the properties and functions of cytochrome b_5 are also summarized.

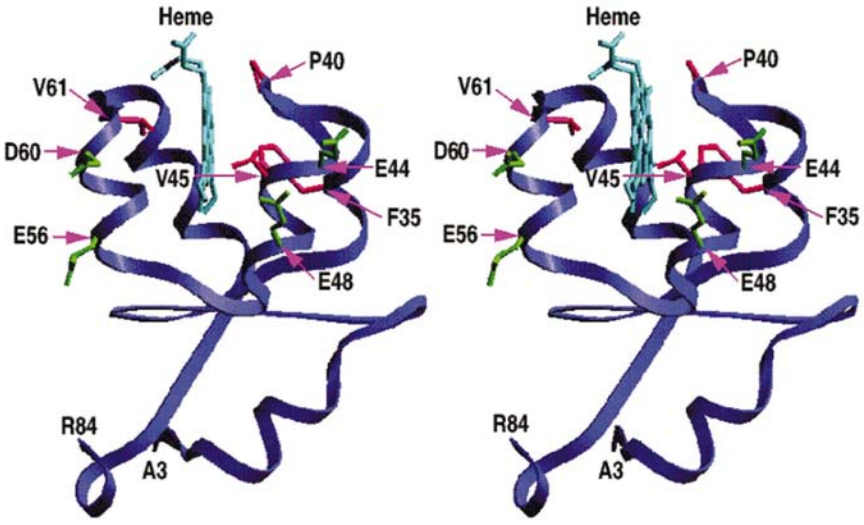

Figure 1
Ribbon diagram of the wild-type Tb_5. The side chains of Phe35, Pro40, Val45 and Val61 are shown in red, and those of Glu44, Glu48, Glu56 and Asp60 in green. Heme is shown in blue. Ala3 and Arg84 are indicated. This diagram was prepared using the program *SETOR* (Evans, 1993).

2. Materials and methods

2.1. Materials

The materials used for the preparation of V45E and V45Y mutants have been reported previously (Wang *et al.*, 2000). The chemicals used for crystallization of the two mutants were of reagent grade.

2.2. Mutagenesis, expression and purification

The purified V45E and V45Y mutants were prepared as reported previously (Wang *et al.*, 2000).

2.3. Crystallization and X-ray data collection

The single crystals of both mutants V45E and V45Y were grown at 293 K in hanging drops using the vapour-diffusion method by mixing 5 µl protein solution

(20 mg ml^{-1}) and 5 µl reservoir solution. The reservoir solution consisted of 3.6 *M* and 3.1 *M* phosphate buffer pH 7.5 for V45E and V45Y, respectively. The crystals grew to a typical size of 0.4 × 0.4 × 0.3 mm within one week. The crystallization conditions are similar to those of the wild-type Tb_5 (Wu *et al.*, 2000).

Diffraction data were collected on a MAR Research Imaging Plate 300 detector system to 1.8 and 1.9 Å resolution for the V45E and V45Y crystals, respectively. The data were processed using the programs *DENZO* and *SCALEPACK* (Otwinowski & Minor, 1997), giving an $R_{\rm sym}$ of 5.1 and 6.2% for V45E and V45Y, respectively. The overall data completeness of both the mutants V45E and V45Y were higher than 93%. The detailed data-collection statistics are shown in Table 1.

2.4. Structure determination and refinement

The structure determination and refinement of both the V45E and V45Y mutants were carried out using the program package *CNS* (Brünger *et al.*, 1998) on a Silicon Graphics Indigo 2 workstation. All data were used to refine the structure except that 10% of the data were randomly selected as a test data set used for monitoring $R_{\rm free}$. Model building was performed using the graphics software *TURBO-FRODO* (Roussel & Cambillau, 1991).

The initial structures of the V45E and V45Y mutants were determined using the difference Fourier method based on the structure of the wild-type Tb_5 at 1.9 Å resolution (Wu *et al.*, 2000) in which the water molecules were omitted and the residue Val45 was replaced by glycine. Rigid-body refinement was carried out at 2.2 Å resolution and the side chains of Glu45 and Tyr45 were fitted to the difference electron-density maps. The structure was then refined for positions and individual thermal parameters for a number of rounds. The coordination geometry of iron was restrained as follows: the distances from Fe to the N atoms NE2 of the axial ligands His39 and His63 were restrained to 2.05 Å and the angle NE2(His39)—Fe—NE2(His63) to 180°.

During the refinement the $(2F_o - F_c)$ and $(F_o - F_c)$ electron-density maps were regularly calculated and used to manually rebuild the model. When the resolution was extended to 2.0 Å, the solvent molecules were gradually included in the model. Only those solvent molecules with temperature factors lower than 50 Å^2 and with reasonable hydrogen bonds to the protein atoms or other solvent molecules were included in the final models at 1.8 and 1.9 Å resolution for V45E and V45Y, respectively.

2.5. Computer modeling

Salemme and Northrup's binding models (Salemme, 1976; Northrup *et al.*, 1993) of the wild-type cytochrome b_5–cytochrome *c* complex were generated by molecular modeling. The manual docking of cytochrome *c* (Bushnell *et al.*, 1990) to Tb_5 (Wu *et al.*, 2000) was carried out on a Silicon Graphics workstation using the graphics software *TURBO-FRODO* and four inter-protein salt bridges were formed for both Salemme's and Northrup's models. The initial model in each binding mode was then energy minimized for 200 cycles, followed by Cartisian molecular-dynamics simulation, during which the integration time was set to 0.005 ps, and 1000 steps were executed at 298 K. Another 200 cycles of energy-minimization were then carried out to generate the final model of the wild-type Tb_5–cytochrome *c* in each binding mode. Based on these models, Val45 was replaced by Tyr45, followed by manual adjustment to avoid unreasonably close contacts to give the initial model of V45Y–cytochrome *c* complex in each binding mode. Starting from each of the initial V45Y–cytochrome *c* models, energy minimization and molecular-dynamics simulation were performed by the same procedure as for wild-type Tb_5–cytochrome *c*, giving the final model of V45Y–cytochrome *c* for each binding mode.

3. Results

3.1. Quality of the V45E and V45Y structures

The *R* factor and $R_{\rm free}$ of the final structure model of the V45E mutant at 1.8 Å resolution are 18.9 and 22.2%, respectively, and those of the V45Y mutant at 1.9 Å resolution are 19.2 and 23.5%, respectively. The r.m.s. deviations of the bond lengths and bond angles from the ideal values are 0.010 Å and 1.08° for the V45E structure, and 0.008 Å and 1.17° for the V45Y structure, respectively. The refinement statistics are shown in Table 1.

The geometry of the two mutant structures was validated using the program *PROCHECK* (Laskowski *et al.*, 1993). All of the non-glycine residues are located within the allowed regions in the Ramachandran plot, with 91.7% in the most favoured regions for both the mutants. The Luzzati plots

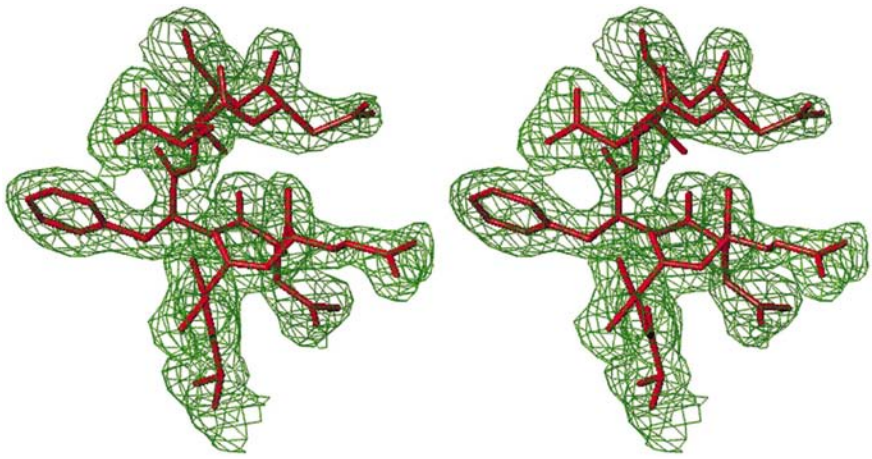

Figure 2
$(2F_o-F_c)$ electron density of α-helix IV of the V45Y mutant, contoured at 1.0σ. This diagram was prepared using the program *TURBO-FRODO*.

(Luzzati, 1952) of V45E and V45Y show that the estimated errors of the atomic coordinates are approximately 0.20 and 0.22 Å, respectively.

Fig. 2 shows, as an example, the electron density of α-helix IV of the V45Y mutant.

3.2. Overall structures

The final model of each asymmetric unit contains 82 amino-acid residues and one heme group as well as 68 and 90 solvent molecules for the V45E and V45Y mutants, respectively.

The secondary structures of both the mutants are the same as that of wild-type Tb_5 (Wu *et al.*, 2000). Each molecule contains six α-helices and one β-sheet composed of five β-strands.

The tertiary structures of the mutants V45E and V45Y are also very similar to that of the wild-type Tb_5, with r.m.s. deviations of 0.11 and 0.16 Å for C^{α} atoms, respectively.

3.3. Local structure around the mutation site

In the wild-type Tb_5 structure, the side chain of Val45 is located at the edge of the heme-binding pocket and points to the heme. Both the C^{γ} atoms of Val45 make van der Waals interactions with heme.

In the two mutants, the volumes of the side chains of both Glu45 and Tyr45 are too large to be accommodated in the hydrophobic pocket, so that they are forced to point into solvent, with the carboxyl group and phenol group outside the hydrophobic pocket. Fig. 3 shows the C^{α} backbones along with the side chains at the residue 45 of the wild-type Tb_5, V45E and V45Y, which are superimposed. The dihedral angle between the heme and the carboxyl group of Glu45 is approximately 45° and the distances from the atoms OE1 and OE2 of the carboxyl group to the heme atoms are 4.17 and 4.94 Å, respectively. The C^{γ} atom of Tyr45 in the V45Y mutant is in the position similar to that of Glu45 in the V45E mutant. The phenol ring of Tyr45 is further from the heme than the Glu45 side chain and the ring plane is almost parallel to the mean plane of the heme.

The C^{α} atoms of Glu45 and Tyr45 are shifted by 0.29 and 0.34 Å, respectively, compared with that of Val45 in the wild-type Tb_5, when the three structures are superimposed. The segment Glu43–Glu44 shifts in both mutant structures and the V45Y mutant shows a larger shift than V45E. The large side chain of Tyr45 is close to the main chain of the segment Gly41–Gly42, resulting in the conformational change of this segment as well in the V45Y mutant. For example, the orientation of the carbonyl group of Gly41 in V45Y differs from that in the wild-type Tb_5 by approximately 10°. Accompanying the shift of the segment Gly41–Tyr45 of helix III in the V45Y mutant, the segment Val61–Gly62, which is located in the other side of heme plane, also makes a corresponding shift of approximately 0.4 Å.

When the main chain of Glu44 is shifted, its side-chain orientation also alters. In the wild-type Tb_5 this side chain fully extends into the solvent and forms an intermolecular hydrogen bond with the side chain of Glu44 of a twofold-axis-related molecule. However, when Val45 is mutated to Glu45 or Tyr45, the side chain of its neighboring residue Glu44 changes orientation and no longer forms a hydrogen bond with the symmetry-related molecule, although it is still exposed to solvent.

Val45 is a non-polar residue located at the edge of the heme-binding pocket and is close to a twofold axis. The distance from Val45 to the symmetry-related molecule is longer than 6 Å in the crystal structure of Tb_5. The side chain of Glu45 of the V45E mutant does not interact with the symmetry-related molecule either, with a shortest distance of 4.5 Å. However, when Val45 is mutated to the much larger residue Tyr45, its hydroxyl group forms a hydrogen bond with the carboxyl group of Glu48 of the twofold-axis-related molecule. The side chain of Glu48 correspondingly rotates by approximately 70° along the $C^{\alpha}-C^{\beta}$ bond in the V45Y crystal structure compared with that in the wild-type Tb_5, in order to facilitate the formation of this hydrogen bond, which is shown in Fig. 4.

A water molecule, Wat240, is found in the V45Y mutant. It is located at the entrance of the heme-binding pocket, also shown in Fig. 4, and forms hydrogen bonds to the main-chain carbonyl O atom of Tyr45 as well as the side chains of Glu48 and Gln49 of the same molecule.

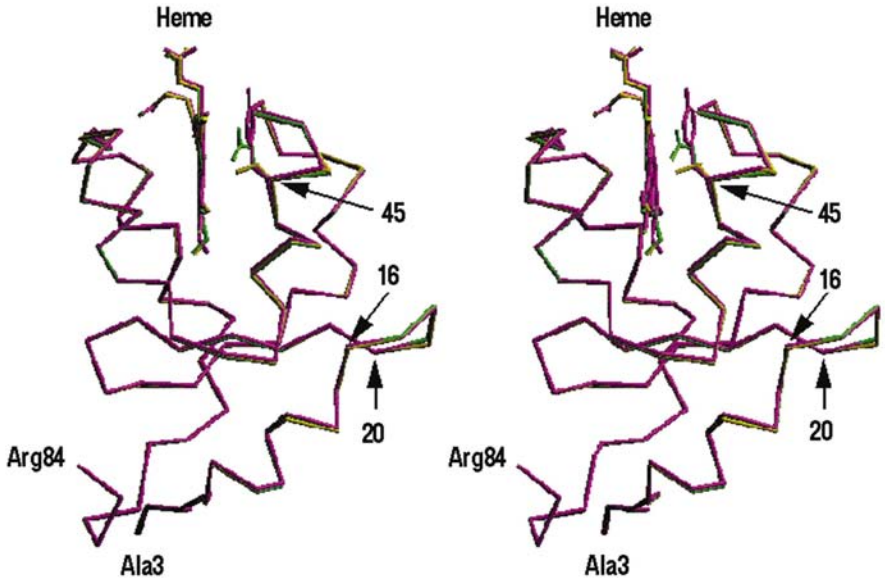

Figure 3
Superimposed C^{α} backbones of the wild-type Tb_5, V45E and V45Y. Ala3 and Arg84 as well as the residues Asn16 and Ser20 are indicated. Heme and the side chains of residue 45 in the three structures are shown. Tb_5, V45E and V45Y are shown in yellow, green and pink, respectively. This diagram was prepared using the program *SETOR*.

Table 2
Structure comparison of the seven mutants and the wild-type Tb_5.

	Tb_5	F35Y	P40V	V45E	V45Y	V61H	E44/56 A	Mut4
Space group	*C*2	*C*2	*C*2	*C*2	*C*2	*C*2	*C*2	$P2_12_12_1$
Unit-cell parameters								
a (Å)	70.70	70.71	70.96	70.91	69.40	70.76	70.69	40.93
b (Å)	40.44	40.39	40.38	40.34	40.44	40.43	40.49	40.88
c (Å)	39.28	39.30	39.43	39.15	39.20	39.31	39.20	52.95
β (°)	111.76	111.72	112.33	111.57	111.70	111.88	111.43	
Resolution (Å)	1.9	1.8	1.9	1.8	1.9	2.1	1.8	1.8
R factor (%)	19.8	19.2	19.3	18.9	19.2	19.2	19.3	19.4
R_{free} (%)	24.8	23.8	23.7	22.2	23.5	24.4	23.2	23.8
R.m.s. deviation of C^{α} (Å) from Tb_5		0.07	0.12	0.11	0.16	0.10	0.08	0.29
Heme binding								
Fe···His39 NE2 (Å)	2.06	2.04	2.09	2.05	2.12	2.11	2.10	2.07
Fe···His39 NE2 (Å)	2.03	2.06	2.04	2.03	2.09	2.08	2.02	2.07
His39 NE2···Fe···His63 NE2 (°)	175.02	176.57	176.34	176.55	175.34	173.37	175.07	177.10

This water molecule does not exist in Tb_5 or V45E. On the other hand, a solvent molecule existing in the wild-type Tb_5 disappears in the V45Y structure because it would be too close to the side chain of Tyr45.

3.4. Heme conformation and orientation

The heme prosthetic group is located in a hydrophobic pocket formed by three β-strands as the bottom and four α-helices as the wall, as shown in Fig. 1. The iron is six-coordinated to four pyrrole N atoms and the NE2 atoms of the two axial ligands His39 and His63. One of the two propionates is hydrogen bonded to Ser64, which shows conserved conformation, and the other extends into the solvent and is more flexible, as indicated by the relatively weaker electron density and higher temperature factor.

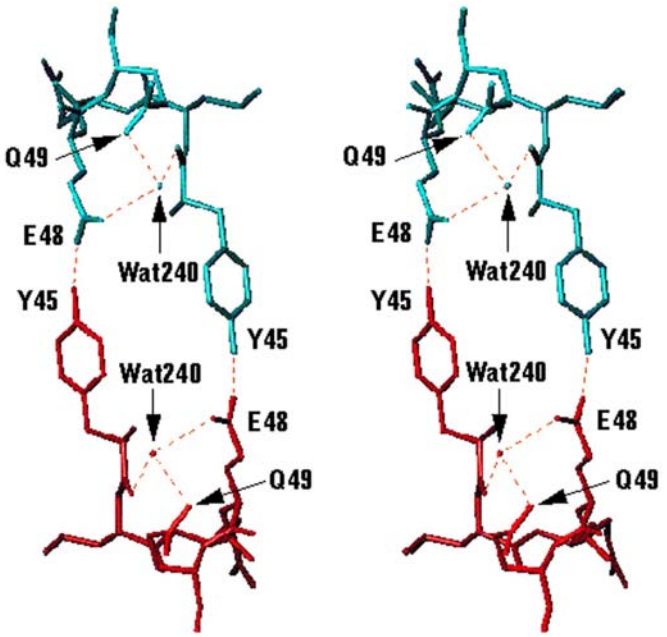

Figure 4
The intermolecular interactions around the mutation site of the V45Y mutant. The residues in the molecule at (x, y, z) are shown in red and those in the symmetry-related molecule at ($-x$, y, $-z$) are shown in blue. Hydrogen bonds are shown in dashed lines. This diagram was prepared using the program *TURBO-FRODO*.

The conformations of the heme and its axial ligands His39 and His63 in the V45E mutant are very similar to those in the wild-type Tb_5. The distances from iron to the NE2 atoms of His39 and His63 are 2.05 and 2.03 Å, respectively, which are also similar to those in Tb_5 (Wu *et al.*, 2000).

However, when Val45 is mutated to the much larger Tyr45, the porphyrin-ring system makes a counter-clockwise rotation of a few degrees about the normal of the mean plane of heme when one looks down on the heme from His63, as shown in Fig. 5(*a*). One of the propionate groups protrudes from pyrrole group A to form a hydrogen bond with Ser64; the axis of the above-mentioned rotation of the porphyrin ring is located approximately at the center of pyrrole ring A. The vinyl group at ring B correspondingly changes orientation so that the position of the atom CBB does not change too much. While the van der Waals contact between CBB and Ser71 C^{β} remains, that between CBB and Leu25 no longer exists, and CBB makes van der Waals contacts with Leu32 in V45Y instead of with Leu25 as in Tb_5. Accompanying the rotation of the porphyrin ring, a conformational change of the axial ligand His39 is observed in the V45Y mutant structure compared with the wild-type Tb_5, *i.e.* the imidazole ring of His39 exhibits a rotation of approximately 10° along the $C^{\beta}-C^{\gamma}$ bond, as shown in Fig. 5(*b*). The side-chain conformation of His63 in the V45Y mutant is basically the same as that in the wild-type Tb_5. The distances from iron to the NE2 atoms of His39 and His63 are 2.12 and 2.09 Å, respectively, which are slightly longer than those in Tb_5 (Wu *et al.*, 2000) and V45E.

3.5. Structure comparison

Table 2 lists the space groups and unit-cell parameters of the wild-type Tb_5 and the seven mutants: F35Y, P40V, V45E, V45Y, V61H, E44/56A and Mut4. The space group of six of the seven mutants is *C*2, the same as that of Tb_5. The only exception is Mut4, in which the tight packing of the molecules cannot be maintained in space group *C*2 because the four long

side chains Glu44, Glu48, Glu56 and Asp60 are mutated to small hydrophobic alanine residues, so that Mut4 crystallizes in a different space group, $P2_12_12_1$. The unit-cell parameter a exhibits an obvious change in the mutant V45Y, being 1.3 Å shorter than that in Tb_5, which can be attributed to the intermolecular interactions of Tyr45 with Glu48 of a symmetry-related molecule, as described above. The tight intermolecular contacts lead to the reduction of the unit-cell parameters. On the other hand, for the P40V mutant the unit-cell parameter β is slightly larger than those of Tb_5 and the other mutants to avoid the unreasonably close contacts between the side chain of Val40 and the Tyr27 of a symmetry-related molecule.

The overall structures of the seven mutants are very similar to the wild-type Tb_5. However, Asn16–Ser20 is a flexible segment (Fig. 3) located at the molecular surface (Durley & Mathews, 1996; Wu *et al.*, 2000), showing a significant difference in conformation in Mut4 from those in the other seven structures. This can be accounted for by the different intermolecular interactions involving this segment, which results from the different crystal packing. The r.m.s. deviations of all the C^{α} atoms of the seven mutants compared with those of the wild-type Tb_5 are shown in Table 2. Mut4 gives the largest r.m.s. deviations.

Table 2 also lists the heme-binding parameters: the distances from iron to the NE2 atoms of the two axial ligands His39 and His63 and the angles His39 NE2—Fe—His63 NE2. No obvious difference is observed based on these data. The heme conformation and orientation are conserved, except those for V45Y which are described above. The conformation of one of the propionates is highly conserved; it is hydrogen bonded to Ser64. The other propionate extends into the solvent and is more flexible, exhibiting a very different conformation in Mut4 from that in Tb_5 and in the other mutant structures, since this propionate is involved in an intermolecular hydrogen-bonding network in space group $P2_12_12_1$, while no such interactions exist in space group $C2$ for the other structures.

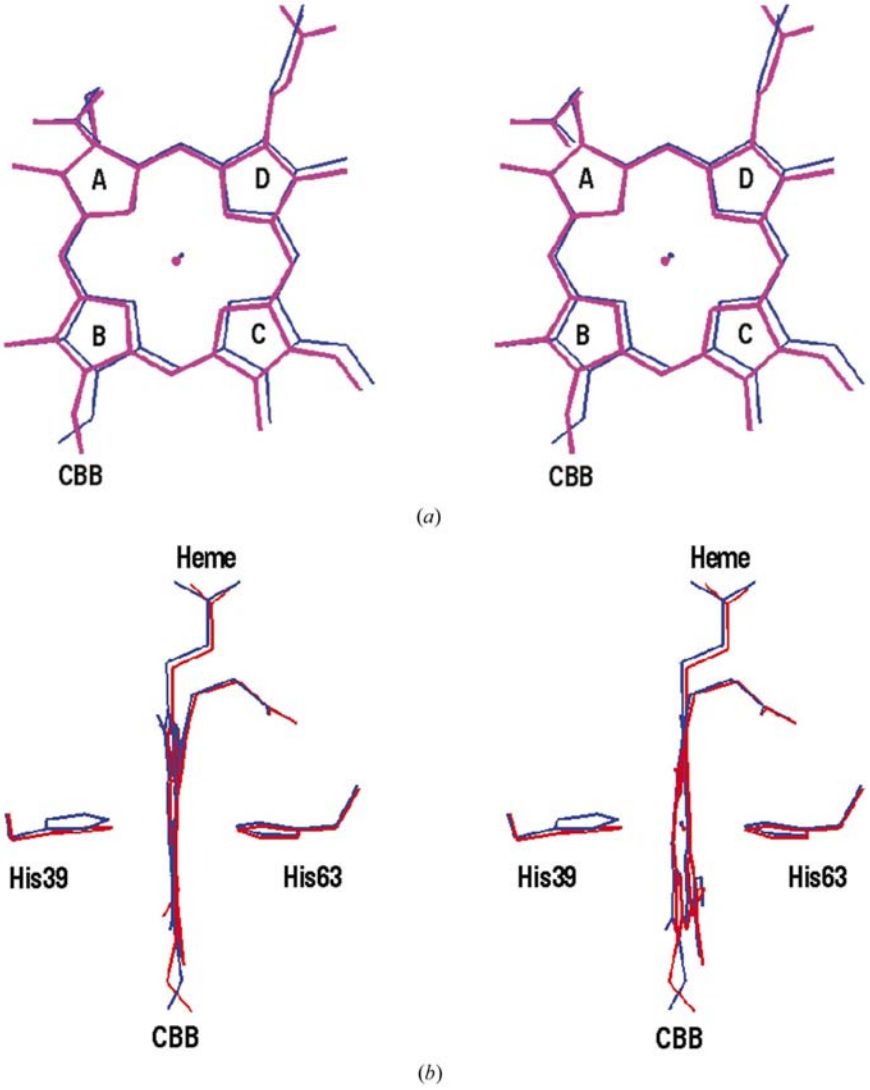

Figure 5
The heme group and the side chains of His39 and His63 of V45Y superimposed with those of the wild-type Tb_5. (*a*) and (*b*) show two different views. The heme of V45Y and wild-type Tb_5 are shown in dark blue and pink, respectively. The pyrrole rings A, B, C and D, and the atom CBB are labeled. These diagrams were prepared using the program *SETOR*.

4. Discussion

Val45 is a residue located at the edge of the hydrophobic heme-binding pocket. The mutation of Val45 to the larger residue Glu45 or Tyr45 influences the properties and functions of cytochrome b_5, such as the redox potential, protein stability, cytochrome b_5–cytochrome c binding constant and electron-transfer rate.

4.1. Redox potential

The redox potentials of the mutants V45E and V45Y are negatively shifted by −23 and −32 mV, respectively, compared with that of Tb_5 (Wang *et al.*, 2000).

The mutation from Val45 to Glu45 introduces a negative charge into the entrance of the heme-binding pocket, which leads to a negative shift of the redox potential of this mutant compared with Tb_5.

In the Tb_5 structure the small and non-polar residue Val45 points towards the heme and forms a 'gate' restricting the access of the solvent molecules into the heme-binding pocket. When Val45 is mutated to the larger residues Glu45 and Tyr45, the side chains cannot be accommodated in the pocket so that they are forced to point into the solvent instead.

The two C^{γ} atom positions of Val45 of Tb_5 are not occupied by any atoms in the two mutants. Thus, in both V45E and V45Y mutants the gate does not exist and a channel is open for the access of the solvent molecules, which is demonstrated by the introduction of a new water molecule, Wat240, in the entrance of the pocket in the V45Y mutant, as described above. Therefore, the hydrophobicity of the heme-binding pocket is reduced by the mutations, which results in a negative shift of the redox potentials of both the mutants compared with Tb_5. Both the carboxyl group of Glu45 and the phenol group of Tyr45 are outside the pocket. The larger volume of the latter causes it to move farther from the heme than the former, as indicated by the smaller dihedral angle between the phenol-ring plane and the mean plane of heme, as shown in Fig. 3. Therefore, the hydrophobicity of the heme-binding pocket in V45Y would be less than that in V45E, leading to the more negative shifts of the redox potentials of V45Y, although the V45E mutant introduces a negative charge and V45Y does not.

4.2. Protein stability

The decrease in the hydrophobicity of the heme pocket of the mutants not only results in a redox-potential change, but also gives rise to a decrease in the stability of the protein towards heat and denaturants such as urea, *i.e.* the heme prosthetic group can be removed more easily from V45E and V45Y than from Tb_5. For example, the transition concentrations of urea (C_m) are 6.8, 5.6 and 4.8 mol l^{-1} for the wild-type Tb_5, V45Y and V45E, respectively (Wang *et al.*, 2000). The stability of the V45E mutant is less than that of the V45Y mutant, which can be attributed to the negative charge of the side chain of Glu45. In the V45E mutant the negatively charged side chain of Glu45 is located right at the entrance of the heme pocket. The electrostatic attraction between the positively charged heme and the negatively charged Glu45 may favour movement of the heme out of the pocket, leading to lower stability of the protein.

4.3. Cytochrome b_5–cytochrome *c* binding

The binding constants of both V45E [0.34 (0.18) $\times 10^6\ M^{-1}$] and V45Y [0.13 (0.03) $\times\ 10^6\ M^{-1}$] are lower than that of Tb_5 [1.13 (0.60) $\times\ 10^6\ M^{-1}$] when they are mixed with cytochrome *c*.

Cytochrome b_5 is an acidic protein and cytochrome *c* is a basic protein, both containing the prosthetic group heme, with negatively and positively charged residues, respectively, distributed at the molecular surface. Salemme and Northrup's binding models (Salemme, 1976; Northrup *et al.*, 1993) illustrate the electrostatic interactions between the two cytochromes. Four salt bridges are formed in each binding model and Glu44 and Glu48 are two of the acidic residues involved in the salt bridges. The side chain of Val45 is close to the binding-interface region and is involved in inter-protein binding through hydrophobic interactions (Guillemette *et al.*, 1994).

Taking Northrup's binding model as an example, Fig. 6 shows the C^{α} backbone of the Tb_5–cytochrome *c* complex model generated by computer modeling, superimposed with the side chains of Glu45 and Tyr45 from the crystal structures of the V45E and V45Y mutants. The mutation of Val45 to Glu45 or Tyr45 introduces a large side chain to the interface of the two proteins and leads to unreasonably close contacts between the two cytochrome molecules. In particular, the very large and rigid side chain of Tyr45 even protrudes into the entrance of the heme pocket of cytochrome *c*, closely contacting with the heme of cytochrome *c*. In order to eliminate these unreasonable contacts the two cytochrome molecules have to change their orientations and move away from each other, which would weaken the binding between them and reduce the binding constants. The computer-generated model of the V45Y mutant–cytochrome *c* complex in Northrup's binding mode reveals that in addition to the salt bridges from Glu48, Glu56, Asp60 and the heme propionate of cytochrome b_5 to Arg13,

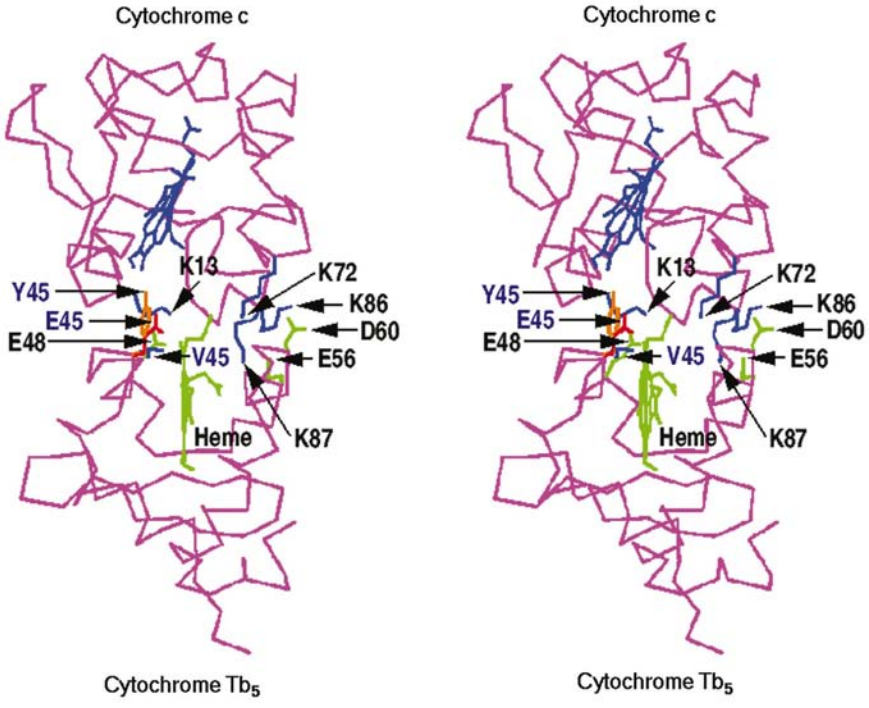

Figure 6
Computer-generated models in Northrup's binding mode of the wild-type Tb_5–cytochrome *c* complex. The C^{α} backbones of Tb_5 and cytochrome *c* are shown in pink. The heme and the side chains involved in the inter-protein salt bridges of Tb_5 are shown in green and those of cytochrome *c* in dark blue. The side chains of Val45, Glu45 and Tyr45 in the crystal structures of Tb_5, V45E and V45Y are superimposed and shown in dark blue, red and orange, respectively. This diagram was prepared using the program *SETOR*.

Table 3
The comparison of the effects of the mutations on the properties and functions of cytochrome b_5.

'+' denotes increase and '−' denotes decrease, compared with the wild-type Tb_5.

Mutants	Redox potential shift (mV)	Stability†	Electron-transfer rate‡
F35Y	−66	+	+
P40V	−40	−	−
V45E	−23	−	−
V45Y	−32	−	−
V61H	+21	−	−
E44/56A	+3	+	−
Mut4	+10	+	−

† The protein stability towards heat and denaturants. ‡ The rate of the electron transfer from cytochrome b_5 to cytochrome *c*.

Lys87, Lys86 and Lys72 of cytochrome *c*, as modeled in the wild-type protein complex (Northrup *et al.*, 1993), the hydroxyl group of Tyr45 forms a hydrogen bond with Gln16 side chain of cytochrome *c*. An energy rise and an increase of approximately 1.2 Å for the inter-iron distance are observed in the V45Y–cytochrome *c* complex compared with those of the modeled Tb_5–cytochrome *c* system.

4.4. Electron-transfer rate

Usually, the redox potential difference between the electron-transfer partners is the driving force for the electron transfer. The redox potentials of V45E and V45Y are negatively shifted compared with Tb_5, so that the electron-transfer rate would be expected to increase. However, the experimental results from stopped-flow spectroscopy reveal that the electron-transfer rates to cytochrome *c* from the mutants are lower than that from the wild-type Tb_5. For example, the electron-transfer rates are 59.9 (2.9) $\times$ 10^6, 54.7 (2.1) $\times$ 10^6 and 66.6 (2.3) $\times$ 10^6 M^{-1} s^{-1} for V45E, V45Y and Tb_5, respectively, at 293 K and an ionic strength of 150 m*M* in phosphate buffer pH 7.0. This fact can be accounted for by the increase of the distance between the two heme groups of cytochrome b_5 and cytochrome *c*, as shown by computer modeling, which results from the introduction of the large side chains to the binding-interface region. This factor is likely to make a greater contribution than the redox potential to the electron-transfer rate.

4.5. Comparison of the effects of various mutations

The effects of the mutations in the seven mutants on the properties and functions of cytochrome b_5 are summarized in Table 3.

F35Y, P40V, V45E, E45Y and V61H are mutants with the mutation sites surrounding the heme. The latter four of the five mutations open a channel for access of the solvent molecules into the heme pocket and decrease the hydrophobicity of the pocket, which results in negative shifts of the redox potentials and a decrease in the stability of the protein towards heat and denaturants. The introduction of a positive charge at the entrance of the pocket in V61H exerts a positive effect on the redox potential greater than the negative effect resulting from the decrease of the hydrophobicity, leading to a final potential shift of +21 mV (Xue *et al.*, 1999). In the F35Y mutant there is sufficient space to accommodate the additional hydroxyl group of Tyr35, so that the local structure at the mutation site in F35Y is basically the same as that in Tb_5. However, the mutation introduces a hydroxyl group pointing towards the edge of the heme group and gives the shortest distance of 3.2 Å from the hydroxyl O atom to a C atom of heme. It greatly reduces the hydrophobicity of the heme pocket, resulting in the largest shift of the redox potential in the negative direction. The van der Waals interactions of the hydroxyl group with heme prevents the heme from moving out of the pocket, so that the stability of this mutant is higher than that of Tb_5. Most of these five mutations give rise to lower electron-transfer rates compared with Tb_5 owing to the lower hydrophobicity of the heme pocket, although the more negative redox potential is favourable for electron transfer. The only exception is F35Y, which shows the largest potential shift in the negative direction, leading to a higher electron-transfer rate than that of Tb_5.

For E44/56A and Mut4, the mutations from the negatively charged surface residues to small non-polar residues give rise to small increases in the redox potential and protein stability. However, these residues are involved in inter-protein binding with cytochrome *c*, therefore the mutations, especially in Mut4, result in an obvious decrease of the binding constants and electron-transfer rates between the two proteins.

This work was supported by National Science Foundation of China (Grant Nos. 39970159, 29731030). We are grateful to Professor Li-Wen Niu, Professor Mai-Kun Teng and Dr Xue-Yong Zhu of the University of Science and Technology of China for their support and help with the X-ray data collection. We acknowledge Professor A. G. Mauk of the University of British Columbia, Canada for his kind gifts of the cytochrome b_5 gene.

References

Brünger, A. T., Adams, P. D., Clore, G. M., Delano, W. L., Gros, P., Grosse-Kunstleve, R. W., Jiang, J. S., Kuszewski, J., Nilges, N., Pannu, N. S., Read, R. J., Rice, L. M., Simonson, T. & Warren, G. L. (1998). *Acta Cryst.* D**54**, 905–921.
Bushnell, G., Louie, G. V. & Brayer, G. D. (1990). *J. Mol. Biol.* **214**, 585–595.
Durley, R. C. E. & Mathews, F. S. (1996). *Acta Cryst.* D**52**, 65–76.
Evans, S. V. (1993). *J. Mol. Graph.* **11**, 134–138.
Guillemette, J. D., Barker, P. D., Eltis, L. D. & Mauk, A. G. (1994). *Biochimie*, **76**, 592–604.
Laskowski, R. A., MacArthur, M. W., Moss, D. S. & Thornton, J. M. (1993). *J. Appl. Cryst.* **26**, 283–291.
Luzzati, P. V. (1952). *Acta Cryst.* **5**, 802–810.
Mathews, F. S. (1985). *Prog. Biophys. Mol. Biol.* **45**, 1–56.
Mathews, F. S., Czerwinski, E. W. & Argos, P. (1979). *The Porphyrins*, Vol. VII, edited by D. Dolphin, pp. 107–147. New York: Academic Press.

Northrup, S. H., Thomasson, K. A., Miller, C. M., Barker, P. D., Eltis, L. D., Guillemette, J. G., Inglis, S. C. & Mauk, A. G. (1993). *Biochemistry*, **32**, 6613–6623.
Otwinowski, Z. & Minor, W. (1997). *Methods Enzymol.* **276**, 307–326.
Roussel, A. & Cambillau, C. (1991). *Silicon Graphics Partners Geometry Dictionary*. Mountain View, CA, USA: Silicon Graphics Inc.
Salemme, F. R. (1976). *J. Mol. Biol.* **102**,563–568.
Wang, Z. Q., Wang, Y. H., Wang, W. H., Xue, L. L., Wu, X. Z., Xie, Y. & Huang, Z. X. (2000). *Biophys. Chem.* **83**, 3–17.
Wu, J., Gan, J. H., Xia, Z. X., Wang, Y. H., Wang, W. H., Xue, L. L., Xie, Y. & Huang, Z. X. (2000). *Proteins Struct. Funct. Genet.* **40**, 249–257.
Xue, L. L.,Wang, Y. H., Xie, Y., Wang, W. H., Qian, W., Huang, Z. X., Wu, J. & Xia, Z. X. (1999). *Biochemistry*, **38**, 11961–11972.